Mechanical characterization of SLID bonded Au-Sn and Cu-Sn interconnections for MEMS packaging

A. Rautiainen, E. Österlund, H. Xu, V. Vuorinen, M. Paulasto-Kröckel

Department of Electrical Engineering and Automation, School of Electrical Engineering, Aalto University, PO Box 13500, FI-00076, Aalto, Finland

ABSTRACT

Several different types of MEMS devices require hermetic sealing for optimal performance and proper functionality. Solid-liquid interdiffusion (SLID) bonding provides the possibility to encapsulate MEMS devices on wafer-level. SLID possess advantages compared to anodic, fusion and metal bonding: 1) possibility to use low process temperature in metal bonding with high re-melting temperature, 2) ductile metals can adopt high stresses and 3) SLID has higher tolerance for topographical variations. In this communication, the mechanical properties of SLID bonded Au-Sn and Cu-Sn based interconnections for MEMS packaging were evaluated with shear and tensile tests. The as bonded samples, composed of Cu-Sn and Au-Sn with Ni-diffusion barrier, exhibited high mechanical strength. Mixed flow gas (MFG) test was used for environmental testing, and the test revealed that Au-Sn samples, with $(Au_5Sn+AuSn)_{eut}$ structure facing the TiW adhesion layer, were susceptible to corrosive environment.

1. INTRODUCTION

Novel interconnection solutions are required to fulfill the continuous need for increasing integration level in electronics packaging. However, the implementation of new materials and processes increases the complexity of interconnection microstructures. This in turn generates challenges in the reliability assessment. To ensure desired functionality and reliability, it is imperative to gain fundamental understanding on the effect of a large variety of design and assembly parameters together with accelerated aging phenomena.

Solid-liquid interdiffusion (SLID) bonding is currently utilized for example in die-attachment of power electronics components [1] and wafer-level hermetic metal bonding for MEMS applications [2-5]. However, in order to utilize this technique more efficiently, or apply it in other applications, more fundamental understanding on the reliability performance is required. Hence, in this communication, wafer-level SLID bonded seal rings for MEMS encapsulation are mechanically characterized and environmentally tested with Mixed flow gas (MFG) test.

2. MATERIALS AND METHODS

Standard double side polished (DSP) 150 mm silicon were utilized as handle wafers, and single side polished (SSP) wafers as cap wafers. The metallization structure of seal rings and the corresponding thicknesses of each layer are presented in Fig. 1.

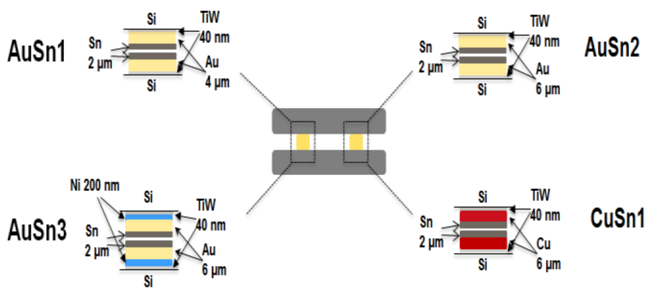

Figure 1. The metallization structure of seal rings and thicknesses of deposited layer

Thin TiW layer was sputtered as an adhesion layer between silicon and seed layer of the SLID bond. In the AuSn3 sample batch, thin Ni layer was sputtered as a diffusion layer. Gold (batches AuSn1-3) and copper (batch CuSn1) layers were sputtered on the front side of both handle and cap wafers. Seal rings' metallization was electroplated to resist openings. The wafers were bonded with EVG501 wafer bonding system in vacuum of 10^{-3} mbar. The process parameters are listed in Tab. 1. After bonding, the wafers were diced into 10x10 mm^2 and 5x5 mm^2 chips.

Table 1. Used bonding parameters

Group	Temperature (K)	Bonding pressure (MPa)	Bonding time (min)
AuSn1	593	2.4	60
AuSn2	593	2.4	60
AuSn3	623	14.4	60
CuSn1	623	14.4	60

Samples for microstructural analysis were prepared using standard metallographic methods. Analysis was performed with JEOL JSM-6330F field emission scanning electron microscope with Oxford Instruments INCA X-sight EDS equipment.

Shear and tensile tests were performed in order to evaluate the bond quality. A special shear test vehicle was utilized for high strength SLID bonds, and stud pull method was used for tensile test. These setups are presented in Fig. 2. Both as bonded samples and samples exposed to corrosive environment were tested with these setups. MTS 858 Table System with Flex Test 40 Digital controller and MTS SilentFlow HPU system was used for force generation and data recording. The constant shear rate was 0,01 mm/s and the tensile load rate was 0,1 mm/s. Average number of tested samples was 5.

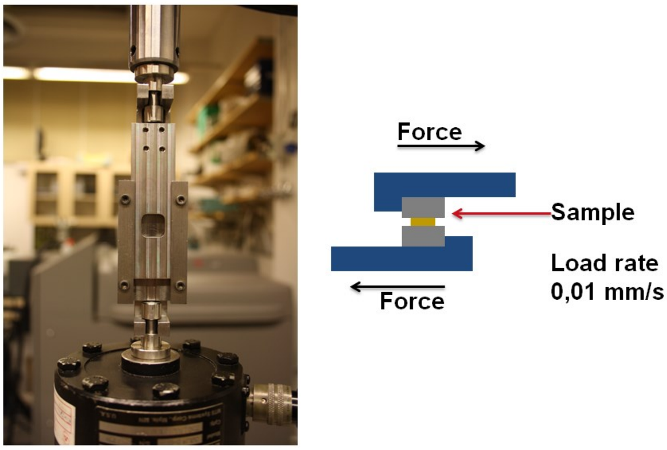

a) Special shear test setup

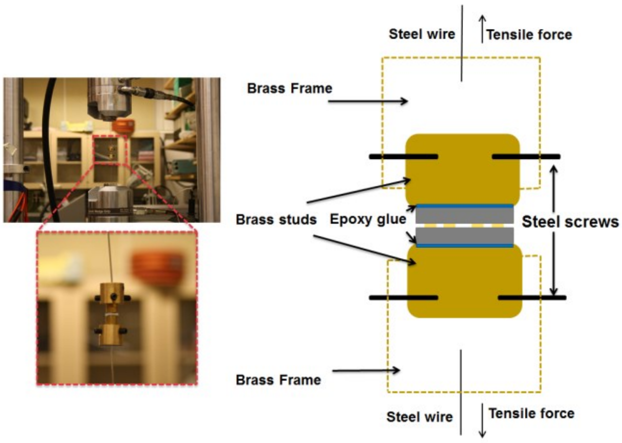

b) Tensile test setup for SLID bonds

Figure 2. Test setups for mechanical characterization of SLID bonds

Weiss WKI1 600/40 Environmental test chamber system was used for the Mixed flow gas test. The MFG test was based on Telcordia GR-63-CORE standard with "Outdoor" conditions [6]. The monitoring of the corrosion environment was conducted according to the ASTM-B810 copper plate mass growth method [7]. The used parameters are listed in Tab.2. The samples from AuSn1 and AuSn2 batches were exposed to maximum 20 days to corrosion environment, and mechanical properties were recorded after every 5 days.

Table 2. Mixed flow gas test parameters

Humidity (%RH)	Temperature (°C)	H_2S (µg/m^3)	NO_3 (µg/m^3)	Cl_2 (µg/m^3)	SO_2 (µg/m^3)
70	30	262	188	19	136

3. RESULTS AND DISCUSSION

3.1. Microstructural analysis

The results from microstructural analysis are presented in Fig. 3. The EDS analysis confirmed the main structure of AuSn1 to be Au_5Sn. However, $(AuSn+Au_5Sn)_{eut}$ structure was found on the edges of the seal ring. For samples from AuSn2 batch, only Au_5Sn was discovered in the analysis. In addition to Au_5Sn structure in AuSn3 samples, thin $(Ni,Au)_3Sn_2$ layer was detected on the both interfaces of the bond. In CuSn1 samples, ~1-3 µm thick Cu layer was detected on both interfaces. The bond composed mainly of Cu_3Sn. Thin TiW was detected in the line scan analysis of all sample batches.

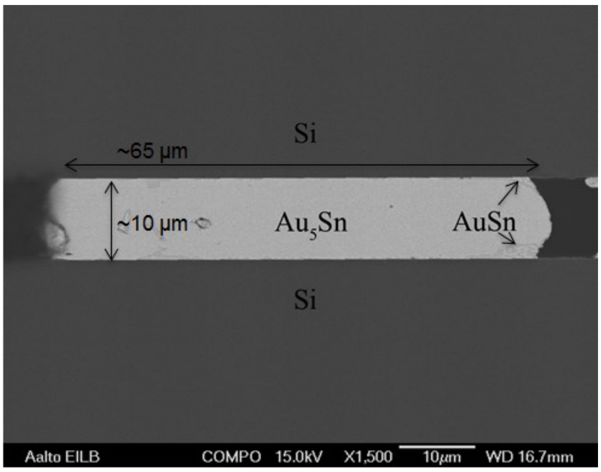

a) Microstructure of as bonded AuSn1 sample

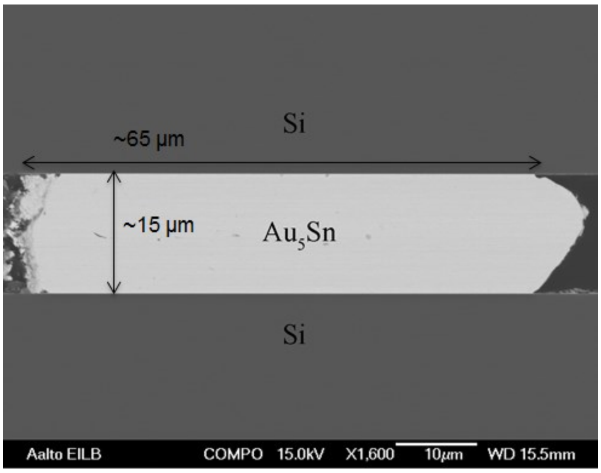

b) Microstructure of as bonded AuSn2 sample

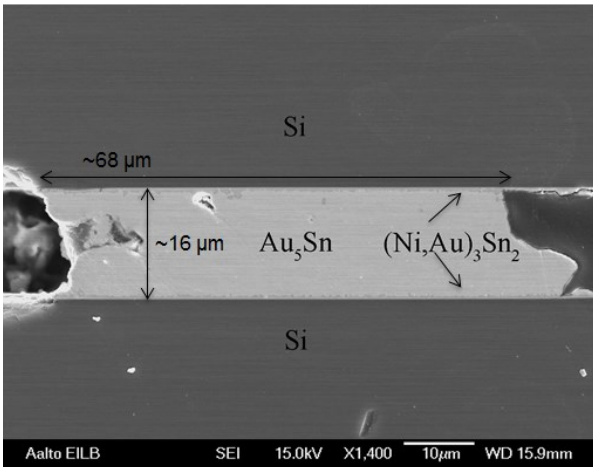

c) Microstructure of as bonded AuSn2 sample

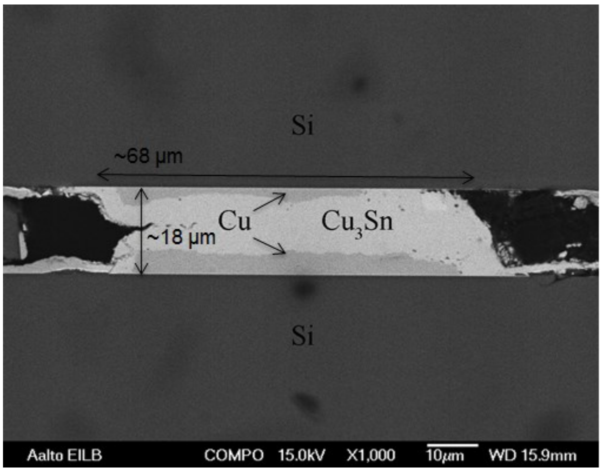

d) Microstructure of as bonded CuSn1 sample

Figure 3. Cross-sectional analysis of as bonded samples

3.2. Mechanical properties

Results from the shear and tensile tests are listed in the Tab 3. Difference in the mechanical properties of

AuSn-based samples can be detected. The shear and tensile strength nearly doubled between AuSn1 and AuSn2. Again, strength increased significantly between AuSn2 and AuSn3. CuSn1 samples exhibited high shear strength, as the tensile strength was in the same scale as with AuSn3 samples. In order to discover the reason for these differences, fracture surface analysis was performed.

Table 3. Results from mechanical tests

	Shear Strength (MPa)	StDev	Tensile Strength (MPa)	StDev
AuSn 1	66	8	24	5
AuSn 2	112	26	41	9
AuSn 3	170	35	88	23
CuSn 1	275	42	91	27

3.3. Fracture surface analysis

Fracture surface of AuSn1 shear tested sample is presented in Fig. 4. $(AuSn+Au_5Sn)_{eut}$ was detected on one side of the failed sample, and TiW was discovered on the corresponding opposite side. Thus, the failure occurs at the interface between adhesion layer and the bond. The same failure mechanism was detected in the analysis of tensile tested samples.

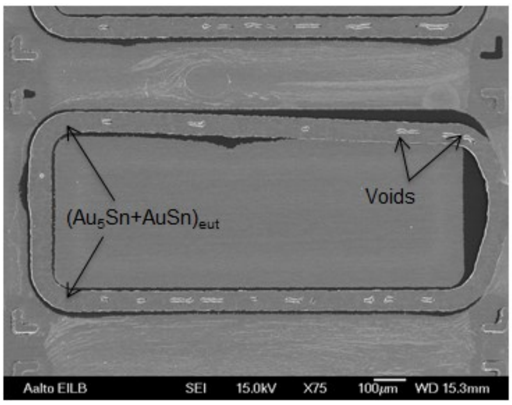

Figure 4. Fracture surface of shear tested AuSn1 sample

With AuSn2 shear tested samples, the fracture surface analysis revealed mixed fracture between TiW-bond interface and cohesive Au_5Sn failure. In the tensile tests, the failure occurred cohesively in the silicon, and some amount of interface failures was observed. Fracture surfaces of shear and tensile tested AuSn2 samples are presented in Fig.5.

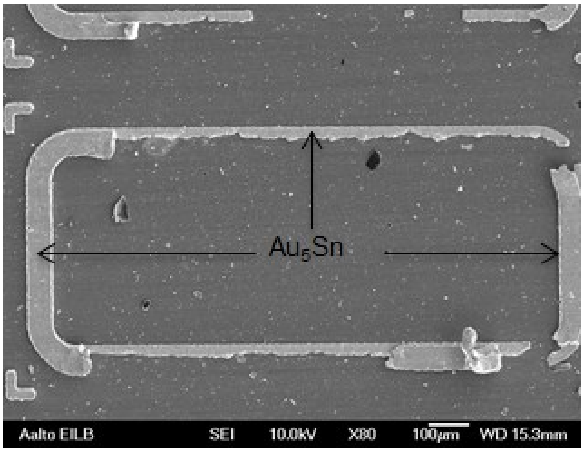

a) Shear tested AuSn2 sample

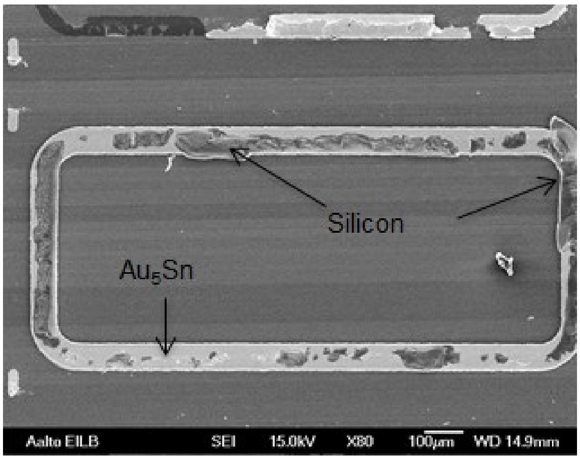

b) Tensile tested AuSn2 sample

Figure 5. Fracture surfaces of AuSn2 samples

Fracture surfaces of AuSn3 shear and tensile tested samples are shown in Fig. 6. After shear test, $(Au,Ni)_3Sn_2$ was detected on one side of the tested sample. Opposite surface contained TiW adhesion layer. Thus, the failure occurred at the TiW-seal ring interface, as with AuSn1 samples. However, in this case, the Ni-barrier indicated to strengthen the interface. In tensile test, the interface between TiW and the seal ring was discovered to be the weakest point.

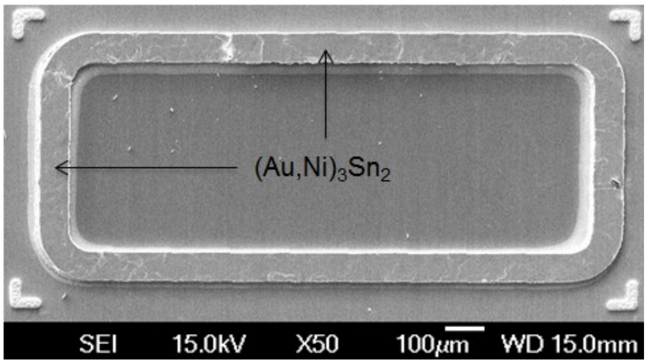

a) Fracture surface of shear tested AuSn3 sample

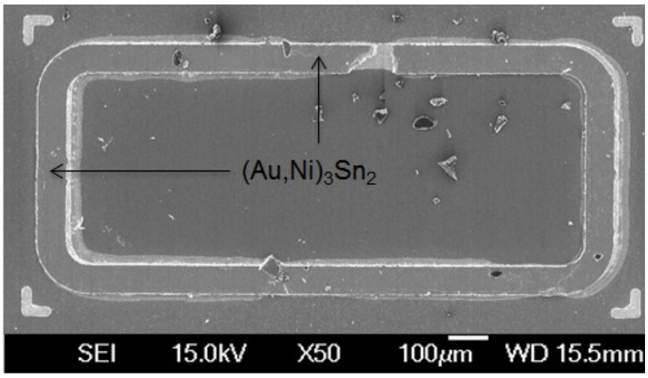

b) Fracture surface of tensile tested AuSn3 sample

Figure 6. Fracture surfaces of shear and tensile tested AuSn3 samples

Fracture surface analysis of shear tested CuSn1 samples exposed a cohesive Cu_3Sn fracture, shown in Fig.7a. In tensile tests, the cohesive silicon fracture was the main failure mechanism, presented in Fig.7b. The high shear strength arises from the cohesive Cu_3Sn fracture. Thus, it is important to have this phase in the bond and the bonding conditions need to be controlled in order to avoid the formation of weak interfaces between different phases such as Cu_6Sn_5 and Cu_3Sn.

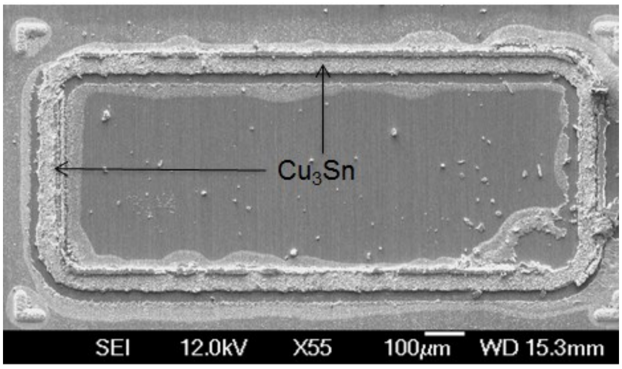

a) Shear tested CuSn1 sample

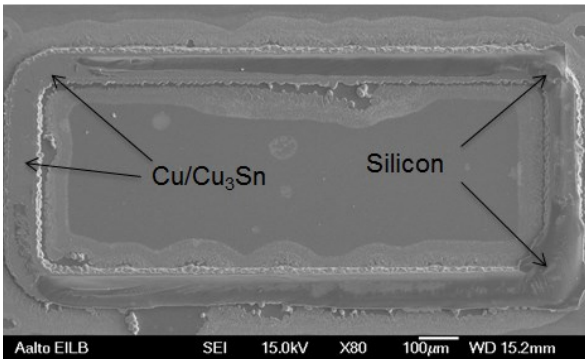

b) Tensile tested CuSn1 sample

Figure 7. Fracture surfaces of shear and tensile tested CuSn1 samples

3.4. Mechanical properties after MFG test

The effect of corrosive environment on Au-based SLID bonds was investigated by evaluating shear and tensile strength after exposing the samples to MFG test. The results are presented in Fig. 8. (AuSn1 samples) and in Fig. 9. (AuSn2 samples).

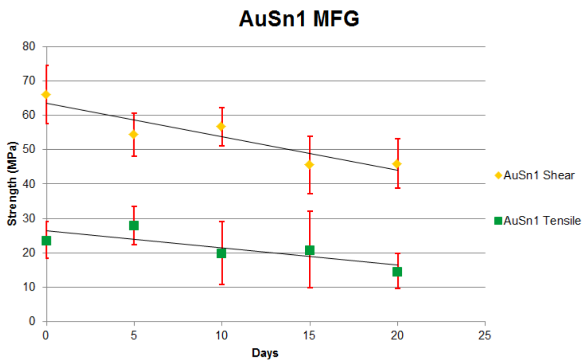

Figure 8. Mechanical properties of AuSn1 samples after MFG test

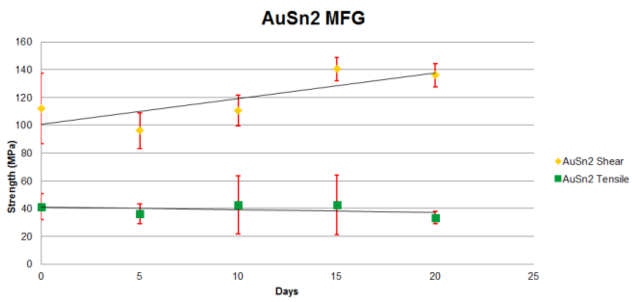

Figure 9. Mechanical properties of AuSn2 samples after MFG test

After 20 days in corrosive environment, the shear strength of AuSn1 samples had reduced ~30%, and the tensile strength reduced ~38%. With AuSn2 samples, results indicate increase in shear strength after 20 days of MFG test. However, taking into account the large deviation of as bonded samples, the increase may not be significant. The tensile strength did not change during the test. The failure mechanisms did not change either in AuSn1 or AuSn2 after MFG test, thus it is assumed that corrosive environment affects on TiW-$(AuSn+Au_5Sn)_{eut}$ interface and reduces the strength. As the structure of the AuSn2 samples was Au_5Sn, it is expected that corrosive environment cannot attack to the interface between the bond and adhesion layer. However, due to the limited amount of samples further investigations are needed confirm these findings.

4. CONCLUSION

In this communication standard thickness silicon wafers were SLID bonded using Cu-Sn and Au-Sn metallizations. The mechanical properties of these interconnections, consisted of intermetallic compounds, were characterized using shear and tensile testing for both as bonded and aged samples. Failure analysis was conducted to rationalize the effects of different interconnections structures on mechanical strength. Cu-Sn samples with Cu-Cu_3Sn-Cu structure exhibited high mechanical strength. Thin Ni diffusion barrier enhanced the mechanical properties of Au-Sn bond. The corrosion environment was found to reduce the strength of Au-Sn seal ring with $(AuSn+Au_5Sn)_{eut}$ structure. However, corrosive environment did not have significant effect on mechanical properties of Au-Sn bond with Au_5Sn structure.

The test results obtained indicate that SLID bondings of Cu-Sn, and Au-Sn with Ni-diffusion barrier, result in highly reliable interconnections. However, it was discovered that different types of manufacturing related defects have a significant effect on the mechanical reliability performance. Cu-Sn bonding possesses high shear and tensile strength, whereas mechanical properties of Au-Sn bondings depend on manufacturing quality and diffusion barrier properties. Au-Sn bonding with Ni barrier demonstrates high shear strength. Also, optimally manufactured void-free Au-Sn, mainly consisted of Au_5Sn, has significantly higher shear strength than Au-Sn consisting of $(Au_5Sn+AuSn)_{eut}$. It was also discovered that non-optimal interfaces, i.e. when $(Au_5Sn+AuSn)_{eut}$ is directly in contact with the TiW adhesion layer, are susceptible to corrosive environments. Especially in Au-Sn system, the results highlight the need to carefully design the thicknesses of metallization layers with respect to the bonding parameters in order to avoid the formation of mechanically weak interfaces and voids.

ACKNOWLEDGEMENTS

The authors would like to thank European Space Agency, the Finnish Funding Agency for Technology and Innovation (Tekes), Okmetic Oyj and Murata Electronics for financial support. One of the authors, Hongbo Xu, appreciates the financial support from Academy of Finland.

References

[1] R. W. Johnson, Cai Wang, Yi Liu and J. D. Scofield, "Power Device Packaging Technologies for Extreme Environments," *Electronics Packaging Manufacturing, IEEE Transactions On,* vol. 30, pp. 182-193, 2007.

[2] Aibin Yu, C. S. Premachandran, R. Nagarajan, C. W. Kyoung, Lam Quynh Trang, R. Kumar, Li Shiah Lim, J. H. Han, Yap Guan Jie and P. Damaruganath, "Design, process integration and characterization of wafer level vacuum packaging for MEMS resonator," in *Electronic Components and Technology Conference (ECTC), 2010 Proceedings 60th,* 2010, pp. 1669-1673.

[3] M. Esashi, "Wafer level packaging of MEMS," *J Micromech Microengineering,* vol. 18, pp. 073001, 2008.

[4] A. Garnier, E. Lagoutte, X. Baillin, C. Gillot and N. Sillon, "Gold-tin bonding for 200mm wafer level hermetic MEMS packaging," in *Electronic Components and Technology Conference (ECTC), 2011 IEEE 61st,* 2011, pp. 1610-1615.

[5] S. Marauska, M. Claus, T. Lisec and B. Wagner, "Low temperature transient liquid phase bonding of Au/Sn and Cu/Sn electroplated material systems for MEMS wafer-level packaging," *Microsystem Technologies,* vol. 19, pp. 1119-1130, 2013.

[6] GR-63-CORE, "GR-63-CORE, Chapter 5.5, "Airborne contaminants test methods," Telcordia Technologies, 2002, 12 p." .

[7] ASTM, "ASTM B810 - 01a(2011): Standard test method for calibration of atmospheric corrosion test chambers by change in mass of copper coupons," ASTM, 2011.